Effect of the initial VDFs in magnetic nozzle expansions

IEPC-2019-818

Presented at the 36th International Electric Propulsion Conference
University of Vienna, Austria
September 15-20, 2019

S. Correyero,* M. Merino† and E. Ahedo‡
Equipo de Propulsión Espacial y Plasmas (EP2), Universidad Carlos III de Madrid, Leganés, 28911, Spain

This work presents a kinetic study of the plasma response in a fully magnetized plasma expansion. A paraxial, collisionless, steady-state plasma model is used to analyze the effect of expanding in a convergent-divergent nozzle a plasma with different types of VDF at the plasma reservoir. The first part of the paper studies the kinetic features, such as magnetic mirroring and anisotropy for both ions and electrons. The collective effects are analyzed by evaluating the momentum and energy equations based on the kinetic solution. The study of the collisionless heat fluxes allows estimating a simple closure to the fluid equation hierarchy for the electrons. The second part of the paper analyzes the solution with two species of electrons with disparate temperatures at the upstream source. A quasineutral steepened profile is formed, which impacts the plasma properties along the expansion. The collisionless electron cooling, as well as the anisotropy on the divergent side of the nozzle are analyzed by separating the different subpopulations of electrons (free, reflected, or doubly-trapped), of both the thermal and the suprathermal species.

I. Introduction

MAGNETICALLY expanding plasmas are present in many different schemes in nature; in magnetic clouds,[1] in laser-induced plasmas,[2] in plasma sources for processing,[3] and in various different ways, in electric propulsion. For instance, the helicon plasma thruster,[4–7] the electron cyclotron resonance thruster,[8] the applied-field magnetoplasma dynamic thruster (AF-MPDT)[9] or the variable specific impulse magnetoplasma rocket (VASIMR)[10] include a magnetic nozzle to expand and accelerate the plasma beam. From a kinetic point of view, the expansion of a magnetically channeled plasma into vacuum involves complex phenomena; for instance, the electron trapping due to the combination of electrostatic barriers with magnetic mirroring.[11–15] The macroscopic effect of the spatial evolution of the distribution functions affects directly the global performance of the nozzle; for this reason, having predictable accurate models of magnetic nozzle expansions is becoming a critical need for the development of the abovementioned thrusters.

In this regard, fluid models are good candidates to obtain quick estimates of the mean plasma properties.[16] However, it is still under discussion the way to close the fluid equation hierarchy. Polytropic cooling laws lack of theoretical justification, and isothermal closures have demonstrated limited value. In this context, Martínez-Sańchez *et al.* developed a steady-state kinetic paraxial model[12] which allowed to compute self-consistently the plasma potential drop along a magnetized slender flow. Merino *et al.* presented later an analogous model for unmagnetized plasma plumes.[13] In both models, an isolated region on the velocity space phase contained a doubly-trapped electron population; electrons disconnected from the upstream source, bouncing between two locations of the divergent side of the expansion due to the combination of magnetic mirroring and electric potential barriers. The distribution function of this population is unknown;

*PhD Candidate, Aeroespace Engineering department, scorreye@ing.uc3m.es
†Associate Professor, Aerospace Engineering department, mario.merino@uc3m.es.
‡Professor, Aerospace Engineering department, eduardo.ahedo@uc3m.es.

in this context, Sánchez Arriaga *et al.* developed a time-dependent kinetic paraxial model to demonstrarte the partial filling during the transient set-up.[17] Moreover, the paraxial approximation used in the above models disregards 2D effects and particle drifts. In a first effort to expand the model in Ref.13 to 2D, Nuez *et al.* have incorporated a fluid-kinetic solution to close the electrons fluid equation hierarchy in a two-fluid 2D magnetic nozzle model,[16] in the fully-magnetized limit.[18]

To remain aligned with the previous studies, in this paper we analyze the kinetic features of a magnetically expanding plasma by thoroughly exploring the kinetic solution of the model in Ref.12, and by modifying the upstream conditions to include different ion and electron distribution functions at the plasma reservoir. In Ref.12, the ions were assumed mono-energetic, and the electrons Maxwellian. These assumptions, in principle suitable for understanding the main features of magnetic nozzle expansions, could fall short of validity to represent the real conditions of the plasma in some devices. For instance, when the expanding plasma consists of two electron populations with disparate temperatures, the ambipolar plasma potential drop could concentrate locally in a thin layer, giving rise to a quasi-neutral steepened layer, or even a double-layer.[19–23]

The rest of the paper is organized as follows.Section II summarizes the main features of the model so the paper is self-explanatory. Section III divides the results in two different cases; first, the solution without suprathermal electrons is presented. The effect of the magnetic mirror combined with the electric potential drop is explained in detail, for both ions and electrons. As well, a fluid description of the plasma is used to validate the kinetic results and analyze the balances in the momentum and energy equations. This will allow to study a possible closure for the fluid equation hierarchy based on the kinetic results. The second part of section III contains the analysis of cases with suprathermal electrons. Advanced results for the development of anisotropy and electron cooling when a small fraction of suprathermal electrons guide the expansion are presented. Finally, the main conclusions are summarized in section IV.

II. Modelling

The steady-state paraxial kinetic model presented here is based on the model described in Ref.12, which is summarized for self-containedness. A plasma source is generated at $z = -\infty$, and expand to $z = \infty$ through a convergent-divergent magnetic nozzle with a single maximum at $z = 0$. The spatial distance z does not appear explicitly in the model, being the non-monotonic magnetic field the independent variable. A convenient, space-like dimensionless variables is therefore defined as

$$\zeta = sign\,(z) \log_{10}\left(\frac{B_M}{B}\right), \tag{1}$$

which places the throat at $\zeta = 0$ and scales logarithmically with B. From here, the spatial distance will be represented by ζ.

The plasma is assumed collisionless and fully magnetized, and therefore both ions and electrons remain attached to the magnetic line. As a direct consequence of these assumptions, all particles conserve their mechanical energy, defined as

$$E = \frac{m}{2}(w_\parallel^2 + w_\perp^2) + eZ\phi, \tag{2}$$

where m and Z represent the particle mass and charge, $w_\parallel$ and $w_\perp$ the parallel and perpendicular components of the particle velocity to the magnetic field lines respectively, ϕ the ambipolar plasma potential, and e the elementary charge.

The particle magnetic moment μ is preserved as an adiabatic invariant.

$$\mu = \frac{m w_\perp^2}{2B}, \tag{3}$$

The model attempts to determine the longitudinal ambipolar plasma potential profile $\phi(\zeta)$, including the finite total potential drop $\phi_\infty = \phi(\infty)$, of a quasi-neutral, current-free plasma beam. It will be assumed (and confirmed by the solution) that $\phi(\zeta)$ decreases monotonically.

By solving Eqs 13 and 3 for $w_\parallel$ and $w_\perp$, and setting $w_\parallel = 0$, one can identify the turning point for particles of given E, μ, or equivalently, the maximum magnetic moment μ_m for a given particle energy E.

$$\mu_m(\zeta, E) = \frac{E - eZ\phi(\zeta)}{B(\zeta)}. \tag{4}$$

This maximum depends on the implicit relation $\phi(B)$, and it is therefore part of the solution.

The axial profile of the maximum magnetic moment will define the type of particles. The ambipolar electric field $\phi(\zeta)$ accelerates ions downstream and confines electrons upstream, while the magnetic mirror effect slows down all particles in the convergent region and accelerates them in the divergent side of the nozzle. These two effects combined lead to different behaviours of ions and electrons. On one hand, for ions the curve μ_m always has a single minimum μ_{iT} in the convergent side at $\zeta = \zeta_{iT}$, which separates *free* from *reflected* particles. On the other hand, electrons are divided into "Low energy" and "High energy". While the curve μ_m for high energy electrons is equivalent to the one for ions but with the minimum μ_{eT} in the divergent side, for low energy electrons more possible topologies are allowed. Both *reflected* and *doubly-trapped* electrons can co-exist in the divergent region. The sketch in Fig. II shows the types of particles allowed in the expansion, which are explained in detail in Ref.12. The remaining regions not specified in Fig. II are void of particles.

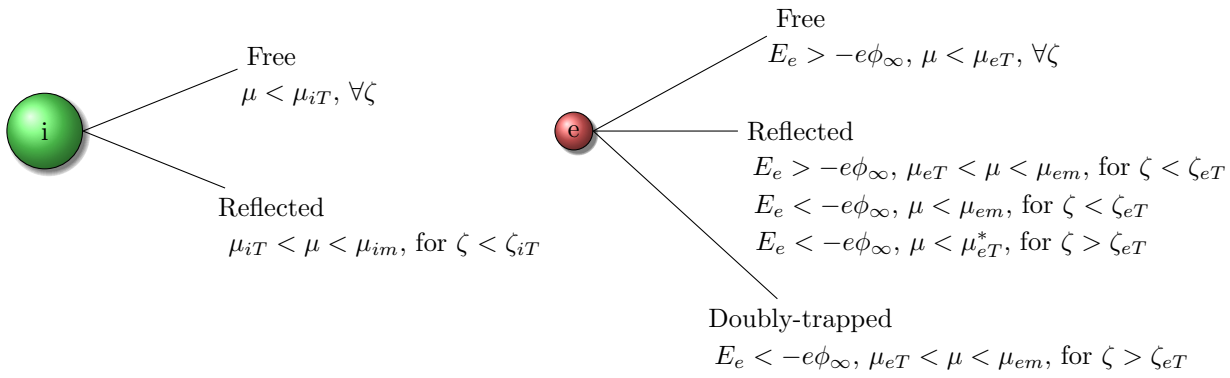

Figure 1. Sketch of the allowed particles in the model with their existence regions. $\mu^*_{eT} \equiv \mu_{eT}$, except for those cases without a local minimum (very low energies), in which $\mu^*_{eT} \equiv \mu_{em}$.

For the boundary conditions of the present study, we assume upstream a mono-energetic or Maxwellian ion distribution function and an electron distribution function consisting of two Maxwellian populations with different temperatures.

$$f_e^+(E_e)dv^3 = \frac{n_{eh*}}{(2\pi)^{3/2}}\left(\frac{m_e}{kT_{eh*}}\right)^{3/2}\exp\left(\frac{-E_e}{T_{eh*}}\right)dv^3 + \frac{n_{ec*}}{(2\pi)^{3/2}}\left(\frac{m_e}{kT_{ec*}}\right)^{3/2}\exp\left(\frac{-E_e}{T_{ec*}}\right)dv^3, \tag{5}$$

with $n_{eh*}, n_{ec*}, T_{eh*}$ and T_{eh*} reference values of density and temperature for each species. The distribution function of the doubly-trapped electrons is assumed to have the same dependence as upstream.

Any macroscopic variable can be computed by integrating directly in the velocity space, or alternatively in E, μ, the distribution function. For any variable χ, this integral is expressed as Eq. 6.

$$\langle\chi\rangle(\zeta) = \frac{2\pi B}{m^2}\int\int d\mu dE \frac{\chi f^+(E)}{|w_\parallel(\zeta,\mu,E)|}, \tag{6}$$

The magnitudes relevant for this work are defined below:

$$\begin{aligned} &n \equiv \langle 1\rangle, \quad nu = \langle w_\parallel\rangle, \quad p_\parallel = nT_\parallel = m\langle c_\parallel^2\rangle, \quad p_\perp = nT_\perp = m\langle w_\perp^2\rangle/2, \\ &q_\parallel = \tfrac{m}{2}\langle c_\parallel^3\rangle = \tfrac{m}{2}\langle w_\parallel^3\rangle - \tfrac{m}{2}nu^3 - \tfrac{3}{2}p_\parallel u, \quad q_\perp = \tfrac{m}{2}\langle w_\perp^2 c_\parallel\rangle = \tfrac{m}{2}\langle w_\perp^2 w_\parallel\rangle - p_\perp u. \end{aligned} \tag{7}$$

The profile of the ambipolar electric potential profile $\phi(\zeta)$ needs to be determined so that current-free and quasineutrality (Eq. 8) conditions are satisfied. Two additional parameters compared to the model in Ref.12 arise from the normalization of the problem: The upstream density ratio of suprathermal electrons $\alpha_0 = n_{eh*}/n_*$, and the upstream temperature ratio between the thermal and the suprathermal populations $\theta_0 = T_{eh*}/T_{ec*}$.

$$\frac{n_i}{n_*} = \alpha_0\frac{n_{eh}}{n_{eh*}} + (1-\alpha_0)\frac{n_{ec}}{n_{ec*}}. \tag{8}$$

An iterative algorithm equivalent to the one in Ref.12 is used to obtain the self-consistent solution of the problem, for a given value of the model parameters. Once the ambipolar potential profile $\phi(\zeta)$ is determined, any moments of the distribution function can be computed, and kinetic and macroscopic features of the expansion can be analyzed.

For the results presented in the following sections, an upstream mean electron temperature is defined as

$$\overline{T}_{e*} = (1-\alpha_0)T_{ec*} + \alpha_0 T_{eh*}. \tag{9}$$

Throughout the expansion, an effective "sonic" velocity is defined as a function of the local density ratio $\alpha = n_{eh}/n_e$,

$$c_{s*} = \sqrt{\frac{1}{m_i\left(\frac{1-\alpha}{T_{ec}} + \frac{\alpha}{T_{eh}}\right)}}. \tag{10}$$

III. Results

A. Case $\alpha_0 = 0$

This section presents the analysis of the plasma response without suprathermal electrons, this is, for $\alpha_0 = 0$. For this case, only two dimensionless parameters drive the problem: the ion to electron mass ratio m_i/m_e and the ion to electron reference temperatures T_{i*}/T_{e*}. Notice that in this case, $T_{e*} = \overline{T}_{e*} = T_{ec*}$. Ions are postulated here as Maxwellian in order to retain asymptotic ion thermal effects. Two solutions are presented, corresponding to "cold" ions, with $T_{i*}/T_{e*} = 0.1$, and "hot" ions, with $T_{i*}/T_{e*} = 10$. The results are analyzed from both a kinetic and a fluid point of view, which allows to obtain a full perspective of the problem.

1. Kinetic analysis

Fig. 2 shows the plasma response for Xenon, with $m_i/m_e = 2.39 \cdot 10^5$. The first row shows the main plasma properties; ambipolar plasma potential and its spatial gradient (a, b), plasma density (c), and ion fluid velocity normalized with $c_{s*} = \sqrt{(T_{e*} + T_{i*})/m_i}$ (d). The plasma potential drop and the final ion velocity are lower for "hot" ions than for "cold" ions. The total potential drop necessary to slow down electrons and fulfill quasi-neutrality and current-free conditions is lower for "hotter" ions, since the ion dynamics is already more similar to the electron's.

The second row of Fig. 2 shows the properties relative to the ions, and the last row the relative to the electrons. A vertical line in the subplots of Fig. 2 indicates the location of the magnetic throat, and therefore separates the convergent from the divergent expansion. In the convergent region, regarding the ion temperatures, while the parallel component drops significantly for both "cold" and "hot" ions, the perpendicular component experiences a dramatic increase for "cold" ions and remains almost unchanged for "hot" ions. This behaviour is the result of the combination of the magnetic mirror effect and the plasma potential drop; while the collective effect of the first one is seen as an increase of the perpendicular temperature in the convergent region which decreases to the source value as it approaches the throat, the plasma potential drop increases the kinetic energy proportionally to T_{e*}. If ions are very energetic, the effect of the plasma potential drop in the convergent region is almost negligible, and therefore the magnetic mirror effect dominates.

In contrast, the electron temperature is almost constant for both cases along the convergent side. In fact, the electron VDF remains Maxwellian and isotropic, except for the small asymmetry due to the "free" electrons. To complement the discussion, Fig. 3 shows the ion and electron VDFs in the $(w_\parallel, w_\perp)$ plane at three spatial locations: the source, the magnetic throat and far downstream. Those particles on the $w_\parallel > 0$ side of the plane that do not have a corresponding image particle on the $w_\parallel < 0$ side are free particles. Regarding ions, the combination of magnetic mirroring with the increase of kinetic energy due to the electric potential drop, explains the shape of the ion VDF shown in Fig. 3. Magnetic mirroring increases $T_{i\perp}$ along the convergent region, but without the effect of the electric potential, it should return to the initial value T_{i*} at the magnetic throat (which is exactly what happens for "hot" ions). However, the electric potential increases the ion kinetic energy, and consequently, opens an empty circular region in the center of ion VDF phase space. For "hot" ions, where $E \gg e\phi$, the effect of the electric potential drop is negligible and therefore

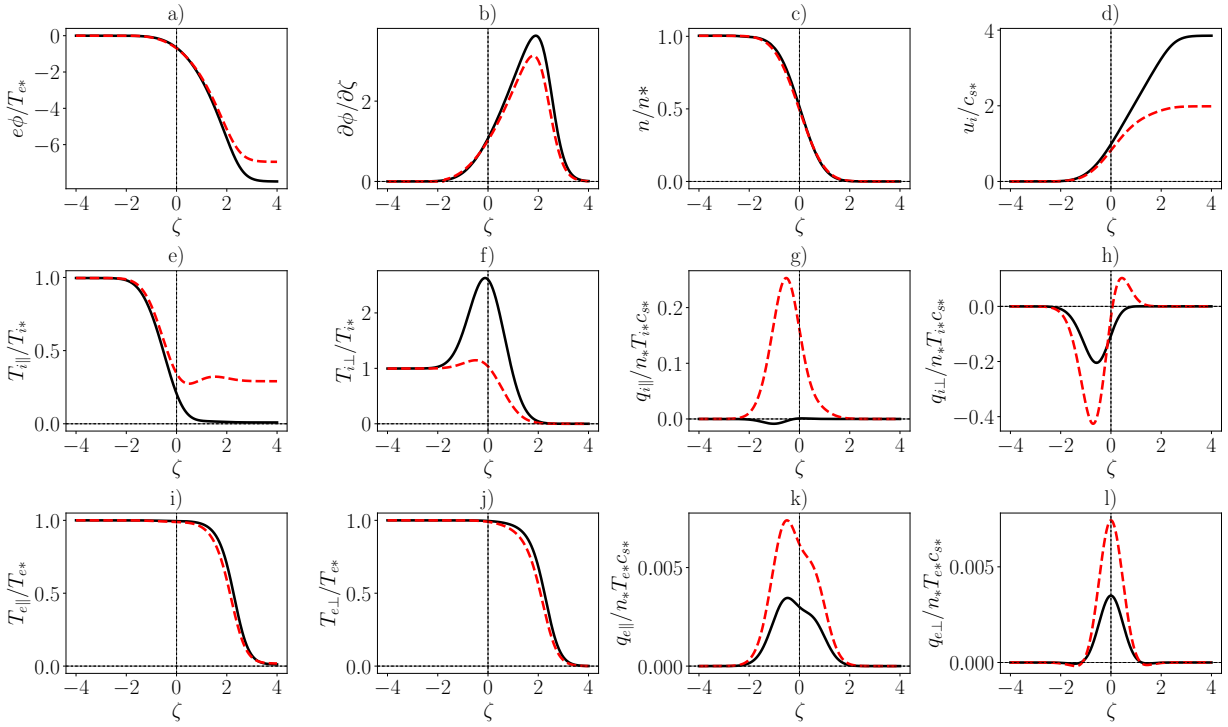

Figure 2. Spatial plasma properties for "cold" ions with $T_{i*}/T_{e*} = 0.1$ (solid) and "hot" ions with $T_{i*}/T_{e*} = 10.0$ (dashed).

only ions feel the magnetic mirror effect in the convergent region. On the contrary, when $E \approx e\phi$, the electric potential drop has a direct impact on the ion VDF. Regarding electrons, Fig. 3 shows that at the throat, contrary to ion VDF, the electron VDF remains almost Maxwellian.

Summarizing, the study of the ion and electron temperatures in the convergent region reveals an interesting character of the expansion: the combination of the magnetic mirror effect and the plasma potential drop is actually felt very differently by ions and electrons; while electrons remain almost Maxwellian and isotropic, ions are strongly affected by magnetic mirroring. Although not plotted here, the developed anisotropy has been found to depend weakly on the mass ratio but largely on T_{i*}/T_{e*}. The expansion dynamics in the convergent region enhances the similarities of the problem with a magnetic cusp, which Martínez-Sánchez and Ahedo studied in Ref. 24 with a very similar model. There, the converging cusp region ended in a wall Debye sheath, while here is followed by the divergent side. The sheath of Ref. 24 and the finite potential drop here have the same function; to confine electrostatically the electron population to fulfill the desired electron current. The present work claims that the assumption taken by Martínez-Sánchez and Ahedo of a near Maxwellian electron VDF in the cusp was actually convenient.

Finally, Figs. 2 g), h), k) and l) show the parallel heat fluxes of parallel and perpendicular energy for ions and electrons. The main feature is their collisionless character, which in principle, appears to be independent of the temperature gradient.

2. Fluid analysis

The following set of equations are the corresponding first direct integrals of the Vlasov equation: continuity, momentum and total energy. Their evaluation allows to perform, not only an independent check of the kinetic results presented in the previous section, but also a complete study of the contribution of the different terms along the expansion.

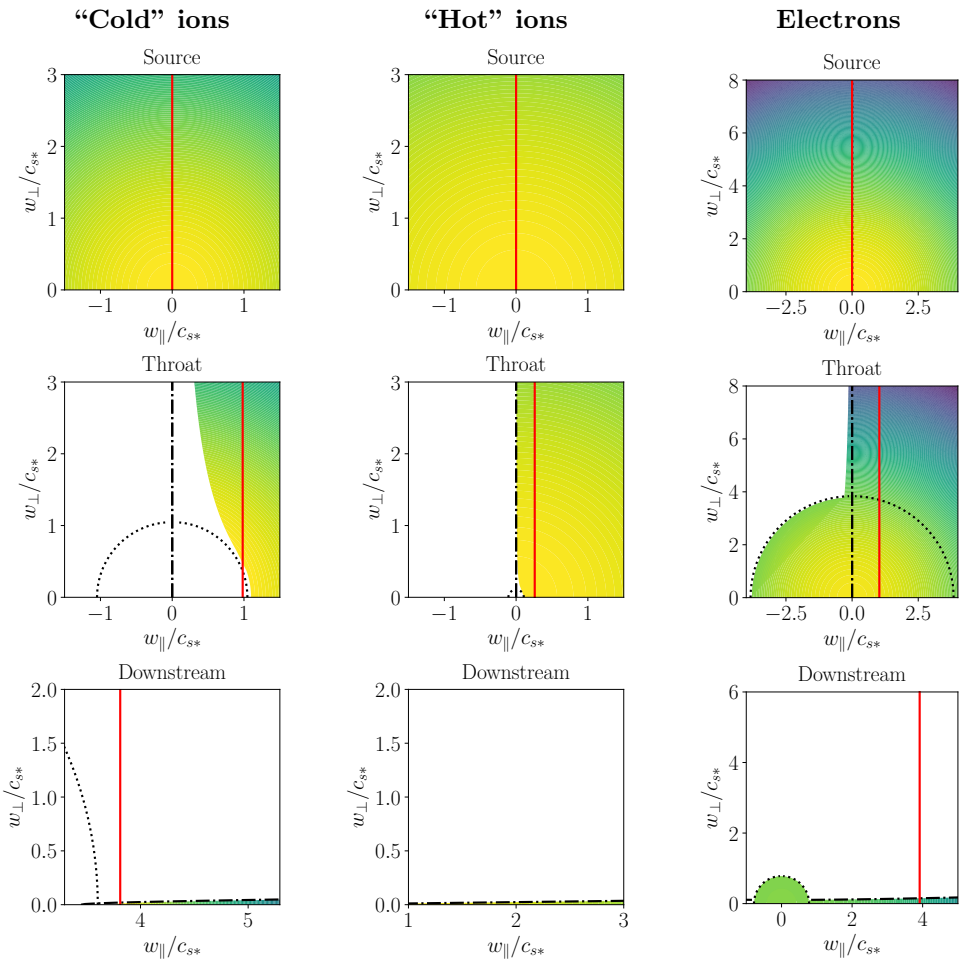

Figure 3. Evolution of the initially Maxwellian ion VDF for $T_{i*}/T_{e*} = 0.1$ (left) and $T_{i*}/T_{e*} = 10$ (center), and the corresponding Maxwellian electron VDF (right). The red vertical solid line indicates the local value of the ion bulk velocity u_i.

$$\frac{nu}{B} = \text{const} \tag{11}$$

$$B\frac{\partial}{\partial\zeta}\left(\frac{mnu^2}{B}\right) + enZ\frac{\partial\phi}{\partial\zeta} + \frac{\partial p_\parallel}{\partial\zeta} - (p_\parallel - p_\perp)\frac{\partial \ln B}{\partial\zeta} = 0 \tag{12}$$

$$\frac{nueZ\phi}{B} + \frac{nu}{B}\left[\frac{mu^2}{2} + \frac{3T_\parallel}{2} + T_\perp\right] + \frac{q_\parallel + q_\perp}{B} = \text{const} \tag{13}$$

$$\tag{14}$$

The continuity equation is verified by the assumptions of the problem and will not be commented upon further. The last term of the momentum equation shows the anisotropy contribution as a volumetric force, which reflects the collective effect of the magnetic mirror phenomenon. Then, the total energy equation shows the balance between the work of the electric field and the contribution of kinetic, thermal, and heat flows.

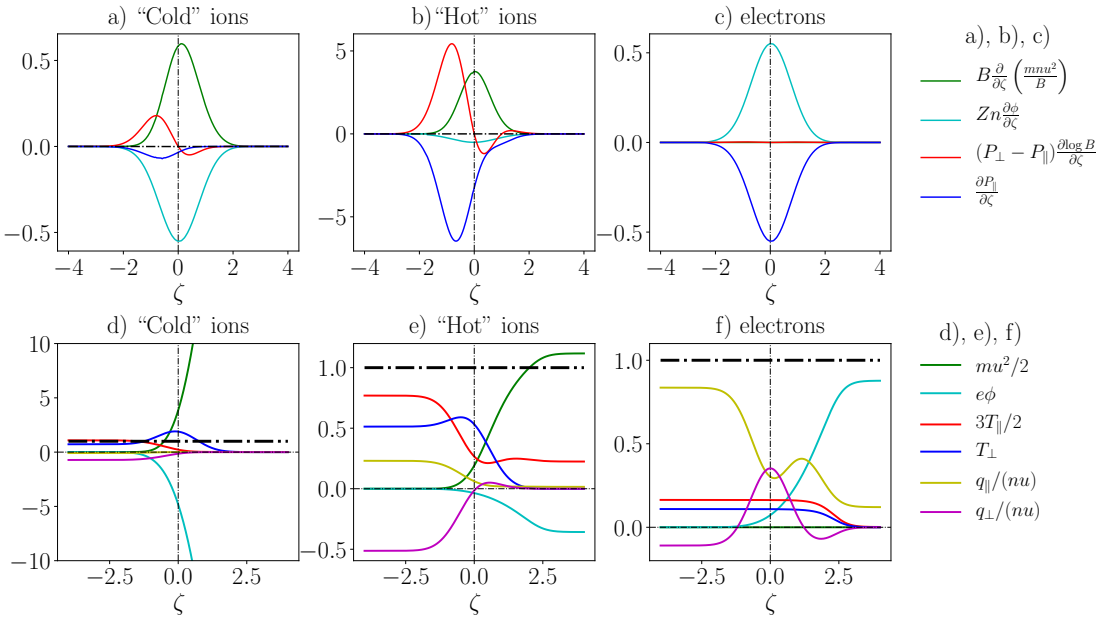

Figure 4. Relative contribution of the different terms to the equations for a),b),c) momentum and d), e), f) total energy. Left plots are for "cold" ions, center for "hot" ions, and right for electrons.

Fig. 4 shows the contribution of the different terms in the momentum and energy equations throughout the expansion, for "hot" ions, "cold" ions and electrons. Regarding the electrons momentum equation, it is confirmed that the inertia term is negligible. Interestingly, the magnetic mirror effect appears to be also negligible even in the divergent side. Therefore, the balance between the electrostatic force and the parallel pressure gradient governs the whole expansion. Regarding ions, a different behaviour has been found for "cold" and "hot" ions. As it was deduced from the kinetic analysis, the electrostatic force has a secondary role in the "hot" ions expansion, being the magnetic mirror effect the dominant term (mainly in the convergent side). Furthermore, this effect together with the pressure gradient, are developed sooner in the expansion compared to ion convection. For "cold" ions, the equilibrium in the momentum equation is mainly between the convective and the electrostatic forces.

Figs. 4 c), d) and e) show the balances in the total energy equation. Upstream, the perpendicular thermal energy flow is balanced with the parallel heat flow of perpendicular energy, and therefore the dominant term is the parallel thermal energy. For "hot" ions, the parallel heat flow also contributes in the upstream source. Along the convergent region, the perpendicular thermal energy gets more dominant, as well as the electric work and the convective terms (but these two last ones almost compensate each other). Finally in the divergent region, while the heat flows vanish for both "cold" and "hot" ions, the parallel thermal flow remains important only for the "hot" ions expansion.

In the electron energy balance, the parallel heat flow has a higher contribution already upstream (it is the dominant term), and remains important throughout all the expansion. In the divergent side, the electric work balances the energy conservation.

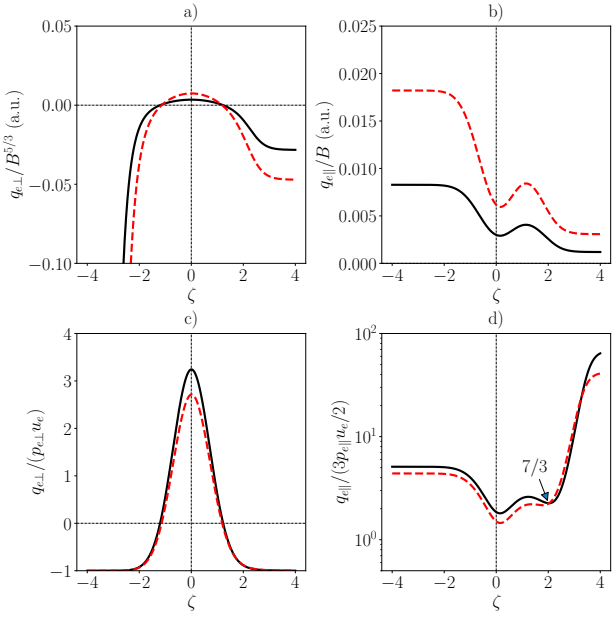

Figure 5. a) $q_{e\perp}$ against $B^{5/3}$ b) $q_{e\parallel}$ against B c) Ratio of perpendicular conduction/convection d) Ratio of parallel conduction/convection. Results are for "cold" ions (solid) and "hot ions (dashed).

In light of these results, it is clear that the CGL double adiabatic limit is not applicable. In addition, a "collisional" closure where the heat flux evolves as the temperature gradient does not fit the results presented here. In order to obtain a proper closure to the fluid equation hierarchy, the conductive and convective terms derived from the kinetic solution are thoroughly analyzed. Fig. 5 shows different ratios involving the parallel fluxes of parallel and perpendicular energy $q_{e\parallel}$ and $q_{e\perp}$. First, Figs. 5 a) and b) show the asymptotic behaviour of both moments, which indeed, agrees with the recent analysis by Ramos[25] *et al.*. Both u_e and $T_{e\ll}$ tend to an asymptotic finite value downstream, and therefore $q_{e\parallel} \propto n_e$, which in turn decays $\propto B$. Then, as Ramos[25] *et al.* showed, when confined electrons dominate the expansion, $T_{e\perp}$ cools down adiabatically, and therefore $T_{e\perp} \propto n^{2/3}$. Since $|q_{e\perp}| \simeq n_e u_e T_{e\perp}$, this leads to $|q_{e\perp}| \propto n_e^{5/3} \propto B^{5/3}$. These asymptotic trends are confirmed by Figs. 5 a) and b).

Finally, Figs. 5 c) and d) show the conductive/convective ratio of perpendicular and parallel fluxes, respectively. The trend of Fig. 5 c) is a direct consequence of Eq. 7. The asymptotic final trend of Fig. 5 d) depends significantly on the initial model parameters (more largely on the ion to electron mass ratio). However, an interesting behaviour has been found in the divergent side, close to $\zeta = 2$; the conductive/convective parallel flux ratio seems to be independent of the initial model parameters, and follows:

$$q_{e\parallel} \approx \frac{7}{2} T_{e\parallel} n_e u_e. \tag{15}$$

This relation has been found for mass ratios $> 10^2$, for both "hot" and "cold" ions, and could be applied to close the fluid equation hierarchy downstream. It must be noticed that the validity of the present model fails for very large ζ, since fully ion and electron magnetization is assumed.

B. Cases $\alpha_0 \neq 0$

1. *Parametric study of α_0 and θ_0*

This subsection analyzes the results of the model described in section II when the upstream electron VDF is formulated as a combination of two Maxwellian populations, with different temperatures. In contrast to subsection A, here the ion population is fixed as a "cold" mono-energetic species. Therefore, this subsection

investigates exclusively the effect of postulating a double Maxwellian distribution function at the upstream source.

A parametric study of the two additional parameters α_0 and θ_0 has been performed for "cold" Xenon ions. Fig. 6 shows the spatial solution with $\alpha_0 = 0.03$ and $\theta_0 = 10$, compared to the equivalent solution without a suprathermal electron population. In the solution with suprathermal electrons, a quasineutral steepened layer (QSL) is formed; both the plasma potential and the fluid velocity show a steep change in the divergent region of the expansion. This change takes place where the suprathermal electrons start dominating the expansion, as it is shown in Fig. 6 d), which represents the ratio between the suprathermal electron density and the local plasma density, $\alpha = n_{eh}/n_e$. The gradient of the electric field, shown in Fig. 6 b), is a good indicator of the exact location of the QSL.

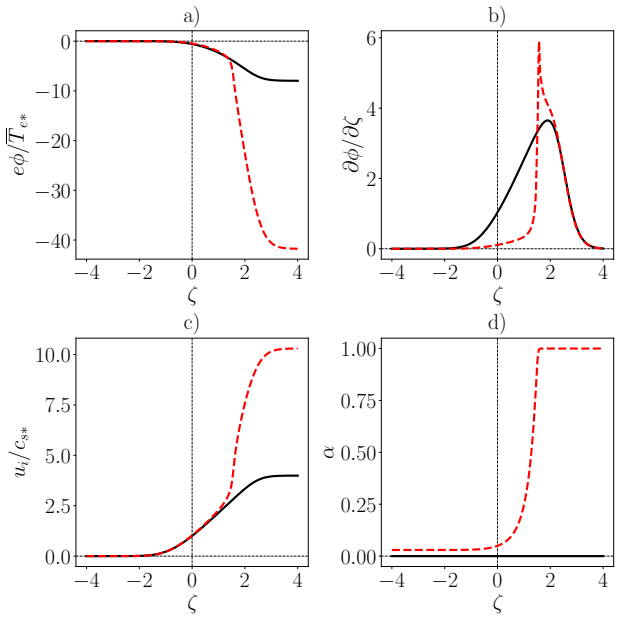

Figure 6. Spatial solution of the model with (dashed) and without (solid) suprathermal electrons ($\alpha_0 = 0.03$ and $\theta_0 = 10.0$). a) Plasma potential, b) Plasma potential gradient, c) Fluid velocity and d) $\alpha = n_{eh}/n_e$

The variation of the QSL location with α_0 shows the same trends found by Ahedo[22] in a three-species convergent-divergent expansion; as α_0 increases, the QSL moves towards the throat. However, in that case the two electron species followed the Boltzmann relation, and therefore, both the ambipolar plasma potential and the final ion velocity were unbounded. The present model obtains the final potential drop as part of the solution, which is shown in Fig. 7 for different values of α_0 and θ_0. The final potential drop is normalized with a mean electron temperature $\overline{T}_{e*}$, defined in Section II, which is equal to T_{ec*} for $\alpha_0 = 0$, and to T_{eh*} for $\alpha_0 = 1$. The value of $e\phi_\infty/\overline{T}_{e*}$ must be the indistinguishable when $\alpha_0 = 0$ and when $\alpha_0 = 1$, and it is confirmed by the solution. Moreover, Fig. 7 a) enables to identify the value of α_0 for which the largest electric potential drop is obtained for the same mean plasma pressure. This value has been found to be $\alpha_{0M} = 0.03$; this is, 3% of the initial electron density belonging to the suprathermal population. Fig. 7 b) shows the total potential drop normalized with the reference thermal electron temperature T_{ec*}. It must be emphasized that the mean electron temperature $\overline{T}_{e*}$ does not assess the propulsive quality of the magnetic nozzle,[22] since the power required to obtain the same $\overline{T}_{e*}$ can be very different. In terms of performance, if we compare all the cases according to the power deposited, including the heat fluxes, all them result in conversion efficiencies very close to 100 %.

2. Behaviour of the two electron species

Once the solution of the model with suprathermal electrons has been analyzed, it is possible to compute the contribution of each subpopulation to any macroscopic variable. Here, we will separate electrons in six subpopulations: thermal free, thermal reflected, and thermal doubly-trapped, suprathermal free, suprathermal reflected, and suprathermal doubly-trapped. To analyze the effect of suprathermal electrons on the

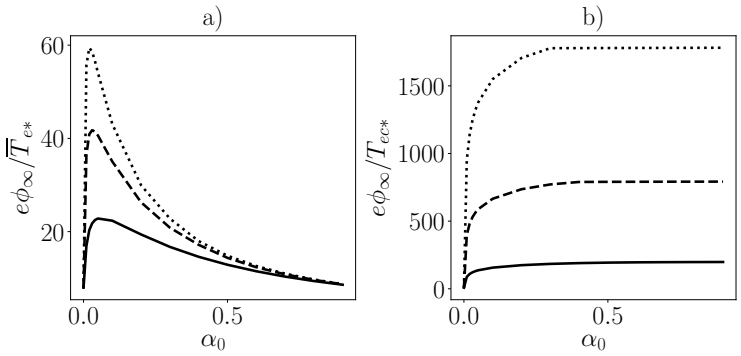

Figure 7. Parametric solution of the final potential drop $e\phi_\infty$, for $\theta_0 = 5$ (———), $\theta_0 = 10$ (- - -) and $\theta_0 = 15$ (-·-·-).

dynamics of the expansion, Fig. 8 shows the contribution of each subpopulation to total density, parallel pressure, and perpendicular pressure, for a solution without suprathermal electrons (left), and for one with $\alpha_0 = 0.03$ (right).

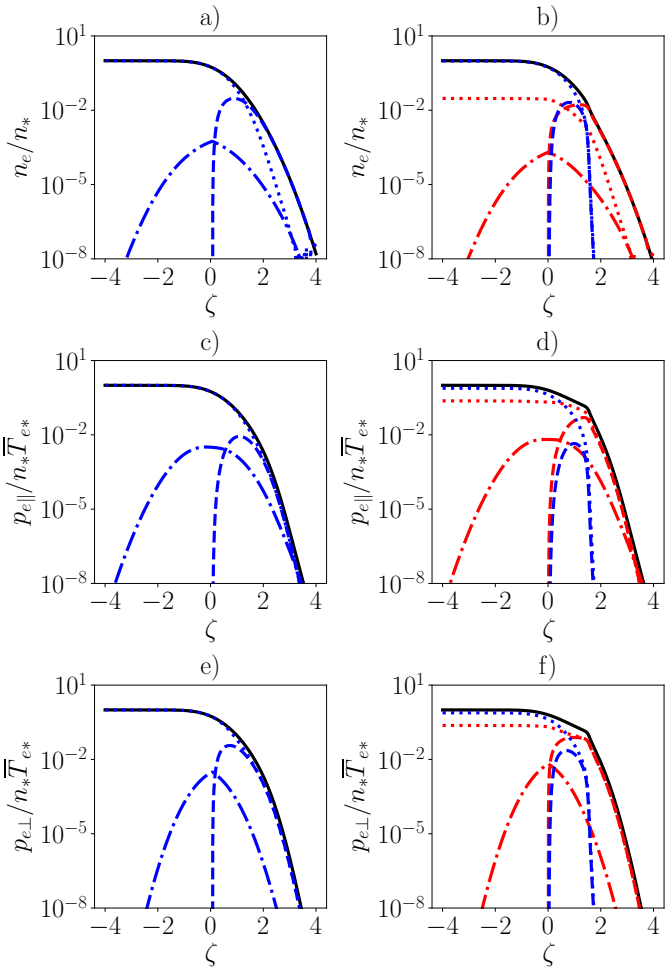

Figure 8. Contribution of the different electron subpopulations to density (a, b), parallel pressure (c, d) and perpendicular pressure (e, f). Suprathermal electrons: free (-·-·), reflected (·····), doubly-trapped (- - -). Thermal electrons: free (-·-·), reflected (·····), doubly-trapped (- - -). Left figures are for $\alpha = 0.0$, while right figures are for $\alpha = 0.03$ and $\theta_0 = 10.0$.

Regarding electron density, without suprathermal electrons, upstream the expansion is driven by the reflected electrons while downstream in the divergent side, the doubly-trapped electrons dominate. This is a direct consequence of assuming a quasi-neutral and current-free solution with large ion to electron mass ratios, as it was shown by Martínez Sánchez *et al.*[12] When there is a small amount of suprathermal electrons, the reflected thermal subpopulation governs the convergent expansion, while at the location of the QSL, the dominant role is switched to the suprathermal doubly-trapped electrons. Specially interesting is the region close to the QSL, where reflected and doubly-trapped, both thermal and suprathermal, have an important contribution to the plasma density. As well, the free thermal electrons do not contribute at all to the electron density, and therefore can be understood as a completely confined population. For larger values of α_0, the change from thermal reflected to suprathermal doubly-trapped electrons takes place sooner in the expansion.

Figs. 8 c) and d) show the contribution to the parallel pressure, which for a solution without suprathermal electrons, is initially governed by the reflected population. In the divergent side, both the reflected and doubly-trapped electrons dominate the expansion, and finally the free electrons contribute most to the parallel pressure. When suprathermal electrons are present, only the reflected subpopulation from the thermal electrons has a significant contribution to the total parallel pressure. As well, the reflected subpopulation of suprathermal electrons can also contribute already to the initial pressure. Finally, Figs. 8 e) and f) show the contribution to the perpendicular pressure. In this case, the free electrons (both thermal and suprathermal) are negligible throughout all the expansion.

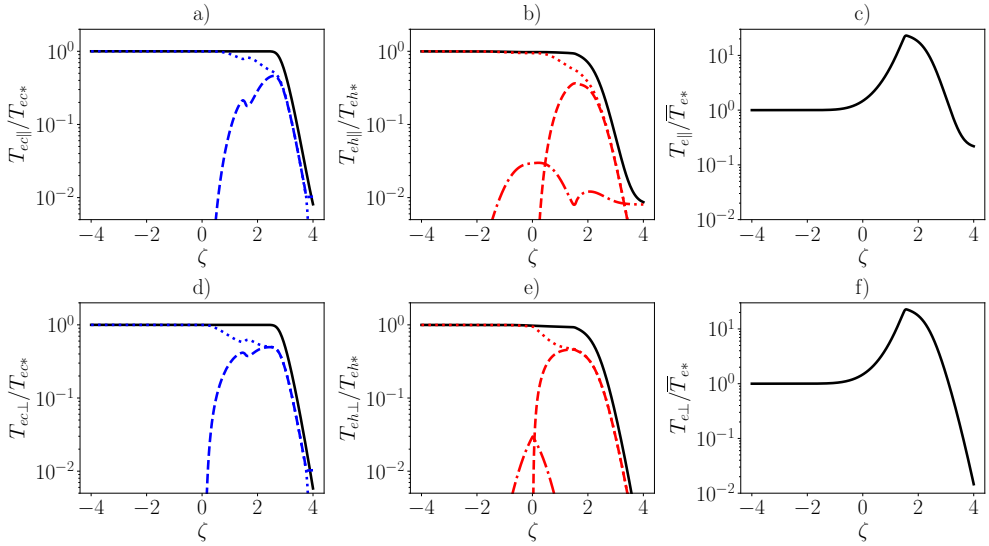

Figure 9. Parallel (a, b, c) and perpendicular (d, e, f) temperatures of the thermal (left) and suprathermal (center) electrons for $\alpha_0 = 0.03$ and $\theta_0 = 10.0$. Suprathermal electrons: free (-·-·-), reflected (·····), doubly-trapped (- - -). Thermal electrons: free (-·-·-), reflected (·····), doubly-trapped (- - -). c) and f) parallel and perpendicular main electron temperatures, respectively.

The contribution of the different subpopulations to both density and pressure are essential to analyze the evolution of the parallel and perpendicular temperatures along the expansion. Fig. 9 shows the temperatures of the thermal and suprathermal populations separately, for $\alpha_0 = 0.03$. The thermal population, which is seen as a completely confined species, remains isothermal and isotropic along almost all the expansion. Only when $\zeta > 3$, the cooling starts to be noticeable. In contrast, the suprathermal population experiences an electron cooling sooner in the expansion, and is also responsible for the anisotropy developed in the divergent side. The total parallel and perpendicular temperatures experience an increase at the location of the QSL, due to the pressure of the Suprathermal electrons, as it is shown in Fig. 9 c) and f).

To close the analysis of the suprathermal electrons, the fluid equations have been applied separately to each species: ions, thermal and suprathermal electrons. Fig. 10 shows the contribution of the different terms to the momentum and energy equations. Fig. 10 a) shows the sharp gain in kinetic energy during the QSL, which is transferred from the parallel pressure gradient of the suprathermal electrons bias the ambipolar electric potential. Again, the anisotropic volumetric force is only important in the convergent side for ions, being almost negligible along all the expansion for electrons. Regarding the energy equation, a

different behaviour has been found for the thermal and suprathermal electrons; upstream, the parallel heat flow is the only dominant term in the thermal electrons energy equation, while the parallel temperature also contributes significantly in the case of the suprathermal electrons energy balance. The situation is different far downstream; the parallel heat flow of the thermal electrons is completely negligible, while it remains significant for the suprathermal ones.

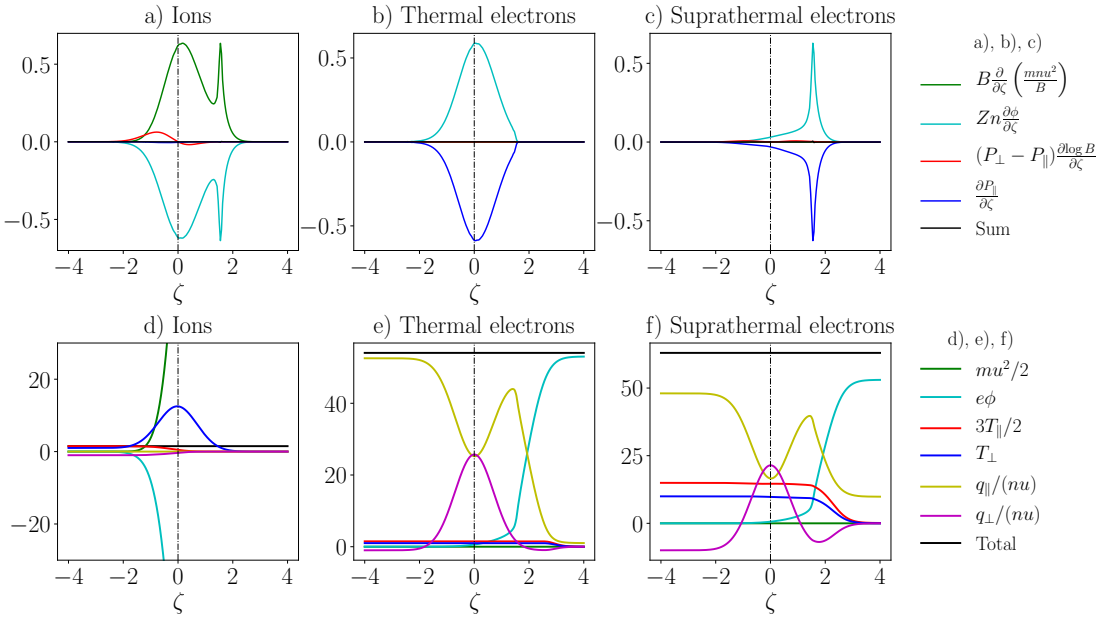

Figure 10. Relative contribution of different terms to the momentum equation for a), b), c) and to the total energy equation d), e) and f). Left plots are for ions, center for thermal electrons and right for suprathermal electrons. Solution is for $\alpha_0 = 0.03$ and $\theta_0 = 10.0$.

IV. Conclusions

This paper presents a kinetic study of a paraxial, collisionless, fully-magnetized, convergent-divergent plasma expansion. Quasi-neutral and current-free solutions have been explored, assuming a known distribution function at the upstream source for both ions and electrons.[12] The electron VDF has been formulated as a combination of two Maxwellian populations, with different temperatures upstream, while the ion VDF is assumed mono-energetic or Maxwellian. With these assumptions, four dimensionless parameters drive the expansion: the ion to electron mass ratio m_i/m_e, the ion to electron source temperature ratio T_{i*}/T_{ec*}, the suprathermal to thermal source density ratio $\alpha_0 = n_{eh*}/n_{ec*}$ and the suprathermal to thermal source temperature ratio $\theta_0 = T_{eh*}/T_{ec*}$. The results presented here correspond to Xenon ions.

The first part of this work analyzes the results for $\alpha_0 = 0$ from a kinetic and a fluid point of view. Two solutions have been presented; for "cold" and "hot" ions, with $T_{i*}/T_{e*} = 0.1, 10$, respectively. It has been showed that ions are strongly affected by magnetic mirroring, while electrons remain almost Maxwellian in the convergent side of the expansion. The effect of the plasma potential drop in the convergent region is weaker for "hot" ions, where the magnetic mirror effect dominates. The similarity of the problem with a converging magnetic cusp has been enhanced.[24] These results enable to define the plasma conditions at the magnetic throat, valuable information for fully-divergent magnetic nozzle models.

The macroscopic analysis of the problem has enable to validate the kinetic solution, showing that momentum and total energy conservation are well satisfied throughout the expansion. Moreover, the evaluation of the fluid equations has shown interesting balances of the different terms. For instance, the anisotropic volumetric force has been found to play a secondary role in the electrons momentum equation, even far downstream; while for ions, its contribution is very significant in the convergent side of the expansion. This part of the work concludes with a study of the internal heat conduction, and its relation with the pressure flux. An interesting behaviour has been found in the divergent side, which has allowed to propose a crude

downstream closure to the fluid equation hierarchy.

Th second part of the paper presents the results for $\alpha_0 \neq 0$. A quasineutral steepened layer (QSL) is formed for small values of α_0. Results are consistent with a previous model by Ahedo[22] with two isothermal electron populations. The value of α_0 which gives the highest potential drop has been found to be $\alpha_{0M} = 0.03$, for the same mean plasma pressure at the source. The thermodynamic behaviour of the two electron species has been analyzed, finding that the thermal population is seen as a confined, isothermal and isotropic ambient plasma throughout almost all the expansion. The anisotropy in the parallel and perpendicular temperatures, as well as the effective electron cooling, are due to the suprathermal electron population thermodynamics, and take place after the QSL.

Acknowledgments

The work has been supported by Project ESP2016-75887 (Spain's National Research and Development Plan - MINECO/FEDER), and by the European Union Horizon 2020 project MINOTOR, that has received funding from the research and innovation program under grant agreement No 730028.

References

[1]V Bothmer and R Schwenn. Eruptive prominences as sources of magnetic clouds in the solar wind. pages 215–220, 1994.

[2]XK Shen, YF Lu, a T Gebre, Hao Ling, and YX Han. Optical emission in magnetically confined laser-induced breakdown spectroscopy. *Journal of Applied Physics*, 100(5):053303, 2006.

[3]M.A. Lieberman and A.J. Lichtenberg. *Principles of plasma discharges and materials processing.* John Wiley and Sons, Hoboken, NJ, 2005.

[4]K. Takahashi, T. Lafleur, C. Charles, P. Alexander, R.W. Boswell, M. Perren, R. Laine, S. Pottinger, V. Lappas, T. Harle, et al. Direct thrust measurement of a permanent magnet helicon double layer thruster. *Applied Physics Letters*, 98:141503, 2011.

[5]R. Winglee, T. Ziemba, L. Giersch, J. Prager, J. Carscadden, and B.R. Roberson. Simulation and laboratory validation of magnetic nozzle effects for the high power helicon thruster. *Physics of Plasmas*, 14(6):063501, 2007.

[6]M.D. West, C. Charles, and R.W. Boswell. Testing a helicon double layer thruster immersed in a space-simulation chamber. *Journal of Propulsion and Power*, 24(1):134–141, 2008.

[7]J Navarro-Cavallé, M Wijnen, P Fajardo, and E Ahedo. Experimental characterization of a 1 kw helicon plasma thruster. *Vacuum*, 149:69–73, 2018.

[8]J. Jarrige, P.Q. Elias, F. Cannat, and D. Packan. Performance comparison of an ECR plasma thruster using argon and xenon as propellant gas. In *33rd International Electric Propulsion Conference*, Paper 2013-420, Washington D.C., October 7-10, 2013. Electric Rocket Propulsion Society, Fairview Park, OH.

[9]A.D. Kodys and E.Y. Choueiri. A critical review of the state-of-the-art in the performance of applied-field magnetoplasmadynamic thrusters. In *41st AIAA Joint Propulsion Conference and Exhibit*, volume 4247, 2005.

[10]F.R.C. Diaz, J.P. Squire, R.D. Bengtson, B.N. Breizman, F.W. Baity, and M.D. Carter. The physics and engineering of the VASIMR engine. In *36th AIAA/ASME/SAE/ASEE Joint Propulsion Conference & Exhibit*, AIAA 2000-3756, 2000.

[11]A.V. Arefiev and B.N. Breizman. Ambipolar acceleration of ions in a magnetic nozzle. *Physics of Plasmas*, 15(4):042109, 2008.

[12]Manuel Martínez-Sánchez, J. Navarro-Cavallé, and E. Ahedo. Electron cooling and finite potential drop in a magnetized plasma expansion. *Physics of Plasmas*, 22(5):053501, 2015.

[13]Mario Merino, Javier Mauriño, and E. Ahedo. Kinetic electron model for plasma thruster plumes. *Plasma Sources Science and Technology*, 27(3):035013, 2018.

[14]JM Little and EY Choueiri. Electron cooling in a magnetically expanding plasma. *Physical Review Letters*, 117(22):225003, 2016.

[15]June Young Kim, Jae Young Jang, KS Chung, Kyoung-Jae Chung, and YS Hwang. Time-dependent kinetic analysis of trapped electrons in a magnetically expanding plasma. *Plasma Sources Science and Technology*, 28(07LT01), 2019.

[16]E. Ahedo and Mario Merino. Two-dimensional supersonic plasma acceleration in a magnetic nozzle. *Physics of Plasmas*, 17(7):073501, 2010.

[17]Gonzalo Sánchez-Arriaga, Jiewei Zhou, E Ahedo, Manuel Martínez-Sánchez, and Jesús José Ramos. Kinetic features and non-stationary electron trapping in paraxial magnetic nozzles. *Plasma Sources Science and Technology*, 27(3):035002, 2018.

[18]Judit Nuez, Mario Merino, and Eduardo Ahedo. Fluid-kinetic propulsive magnetic nozzle model in the fully magnetized limit. In 36^{th} *International Electric Propulsion Conference*, number IEPC-2019-254, Vienna, Austria, 2019. Electric Rocket Propulsion Society.

[19]S.A. Cohen, X. Sun, N.M. Ferraro, E.E. Scime, M. Miah, S. Stange, N.S. Siefert, and R.F. Boivin. On collisionless ion and electron populations in the magnetic nozzle experiment (MNX). *IEEE Transactions on Plasma Science*, 34(3):792–803, 2006.

[20]C. Charles. A review of recent laboratory double layer experiments. *Plasma Sources Science and Technology*, 16:1, 2007.

[21]Eduardo Ahedo and Manuel Martínez Sánchez. Theory of a Stationary Current-Free Double Layer in a Collisionless Plasma. *Physical Review Letters*, 103(13):1–4, 2009.

[22]Eduardo Ahedo. Double-layer formation and propulsive assessment for a three-species plasma expanding in a magnetic nozzle. *Physics of Plasmas*, 18(3):033510, 2011.

[23]Mario Merino and E. Ahedo. Two-dimensional quasi-double-layers in two-electron-temperature, current-free plasmas. *Physics of Plasmas*, 20(2):023502, 2013.

[24]Manuel Martínez-Sánchez and E. Ahedo. Magnetic mirror effects on a collisionless plasma in a convergent geometry. *Physics of Plasmas*, 18(3):033509, 2011.

[25]Jesús Ramos, Mario Merino, and E. Ahedo. Three dimensional fluid-kinetic model of a magnetically guided plasma jet. *Physics of Plasmas*, 25(6):061206, 2018.